Title:

Prediction of H3K27M alteration status in brainstem glioma using multi-shell diffusion MRI metrics

Manuscript Type: Research Article

Author list: Xiaolu Xu MD, PhD[1*]; Peng Zhang, MD, PhD[2*]; Zhizheng Zhuo, PhD[1]; Yunyun Duan, MD, PhD[1]; Liying Qu, MS[1]; Dan Cheng, MD[1]; Ting Sun, PhD[1]; Jinli Ding, PhD[1]; Cong Xie, MS[1]; Xing Liu, MD, PhD[3]; Sven Haller, MD, PhD[4]; Frederik Barkhof, MD, PhD[5,6]; Chuyang Ye, PhD[7]; Liwei Zhang, MD, PhD[2]; Yaou Liu, MD, PhD[1]

Authorship

*Xiaolu Xu and Peng Zhang contributed equally to this study.

Affiliation:

1. Department of Radiology, Beijing Tiantan Hospital, Capital Medical University, Beijing, China, 10070

2. Department of Neurosurgery, Beijing Tiantan Hospital, Capital Medical University, Beijing, China, 10070

3. Department of Pathology, Beijing Tiantan Hospital, Capital Medical University, Beijing, China, 10070

4. Department of Imaging and Medical Informatics, University Hospitals of Geneva and Faculty of Medicine of the University of Geneva, Geneva, Switzerland

5. UCL Institutes of Neurology and Healthcare Engineering, London, UK

6. Department of Radiology & Nuclear Medicine, Amsterdam University Medical Centers, The Netherlands

7. School of Information and Electronics, Beijing Institute of Technology, Beijing, China

Corresponding to: Yaou Liu, MD, PhD, Department of Radiology, Beijing Tiantan Hospital, Capital Medical University. No.119, the West Southern 4th Ring Road, Fengtai District, Beijing, 100070, China. Tel: 86- 13810345782; Fax: 86 10 59975358. E-mail: liuyaou@bjtth.org.

Funding:

Y.L is supported by the National Science Foundation of China (No. 81870958), the Beijing Municipal Natural Science Foundation for Distinguished Young Scholars (No. JQ20035), the Special Fund of the Pediatric Medical Coordinated Development Center of Beijing Hospitals Authority (No. XTYB201831).

F.B is supported by the NIHR biomedical research center at UCLH.

Conflict of Interest: All authors reported no competing interests.

Running title:

H3K27M identification by diffusion MRI

Abstract

BACKGROUND

Multi-shell diffusion characteristics may help characterize brainstem gliomas (BSGs) and predict H3K27M status.

PURPOSE

To identify the diffusion characteristics of BSG patients and investigate the predictive values of various diffusion metrics for H3K27M status in BSG.

STUDY TYPE

Prospective.

POPULATION

Eighty-four BSG patients (median age 10.5 years [IQR 6.8-30.0 years]) were included, of whom 56 were pediatric and 28 were adult patients.

FIELDSTRENGTH/SEQUENCE:

3T, multi-shell diffusion imaging.

ASSESSMENT

Diffusion kurtosis imaging (DKI) and neurite orientation dispersion and density imaging (NODDI) analyses were performed. Age, gender and diffusion metrics, including fractional anisotropy (FA), mean diffusivity (MD), axial diffusivity (AD), radial diffusivity (RD), mean kurtosis (MK), axial kurtosis (AK), radial kurtosis (RK), intracellular volume fraction (ICVF), orientation dispersion index (ODI) and isotropic volume fraction (ISOVF), were compared between H3K27M-altered and wildtype BSG patients.

STATISTICAL TESTS

Chi-square test, Mann-Whitney U test, multivariate analysis of variance (MANOVA), step-wise multivariable logistic regression. P-values<0.05 were considered significant.

RESULTS

82.4% pediatric and 57.1% adult patients carried H3K27M alteration. In the whole group, the H3K27M-altered BSGs demonstrated higher FA, AK and lower RD, ISOVF. The combination of age and median ISOVF showed fair performance for H3K27M prediction (AUC = 0.78). In the pediatric group, H3K27M-altered BSGs showed higher FA, AK, MK, ICVF and lower RD, MD, ISOVF. The combinations of median ISOVF, 5th percentile of FA, median MK and median MD showed excellent predictive power (AUC = 0.91). In the adult group, H3K27M-altered BSGs showed higher ICVF and lower RD, MD. The 75th percentile of RD demonstrated fair performance for H3K27M status prediction (AUC = 0.75).

DATA CONCLUSION

Different alteration patterns of diffusion measures were identified between H3K27M-altered and wildtype BSGs, which collectively had fair to excellent predictive value for H3K27M alteration status, especially in pediatric patients.

Keywords

Brainstem glioma, H3 K27M alteration, multi-shell diffusion, diffusion kurtosis imaging, neurite orientation dispersion and density imaging

Introduction

Brainstem gliomas (BSGs) represent a group of heterogeneous tumors with variable biological behavior occurring in the midbrain, pons, and/or medulla oblongata. These tumors account for 4.2% of primary brain and other central nervous system gliomas, and are more commonly seen in children[1]. Pediatric BSG patients exhibit a different clinical presentation and prognosis compared to their adult counterparts, indicating a possibly different pathogenesis[2-4].

The WHO 2021 classification of CNS tumors is heavily weighted toward molecular diagnosis[5]. H3 K27M alteration is the most frequent mutation in BSGs and is predominantly detected in pediatric patients. The mutation is caused by a lysine-to-methionine substitution at amino acid position 27 in histone H3[6], and is crucial for optimal diagnosis, appropriate treatment and outcome prediction[5]. To stay relevant, imaging should also focus on identifying molecular status.

While other imaging modalities focus on macroscopic volume or functional (e.g., metabolic and vascular) changes, diffusion-weighted magnetic resonance imaging (e.g., diffusion weighted imaging [DWI], diffusion tensor imaging [DTI], diffusion kurtosis imaging [DKI], neurite orientation dispersion and density imaging [NODDI]) allows studying microstructural changes in BSGs. Diffusion MR techniques have been used as a non-invasive, quantitative method to depict cellular profiles of gliomas[7-9], and previous studies suggested diffusion metrics hold promise to predict genetic (e.g., isocitrate dehydrogenase [IDH]) mutation status [10-12].

Currently, little is known about the diffusion characteristics of BSGs and their potential value to determine H3 K27M alteration status. Therefore, we studied the advanced diffusion characteristics of BSG patients using comprehensive multi-shell diffusion

analysis (DTI/DKI/NODDI), and investigated the predictive values of various diffusion metrics for H3 K27M alteration status in BSG at large and in subgroups of pediatric and adult patients.

Materials and Methods

Participants

This study was approved by the Institutional Review Board of Beijing Tiantan Hospital, Capital Medical University, Beijing, China. Written informed consent was obtained from all participants or their legal surrogates according to the Declaration of Helsinki.

Patients with BSGs were prospectively recruited between December 2018 and December 2020 at Beijing Tiantan Hospital, Capital Medical University. The inclusion criteria were (1) complete preoperative multi-shell diffusion MRI examinations; (2) confirmed histological diagnosis of brainstem glioma; (3) availability of H3K27M molecular status information, either H3 K27M-altered or wild-type. The exclusion criteria were (1) incomplete or low-quality MRI images, (2) declination of participation by the patients. Clinical variables such as age and gender were recorded.

Pathological analysis

Tumor grading was performed by an experienced pathologist (X.L, with five years' experience in pathology) according to the 2016 World Health Organization Classification of Tumors of the Central Nervous System[13]. H3K27M alteration status (H3K27M-altered or wildtype) was determined by immunohistochemical (IHC) analysis using a mutation-specific antibody (Merck Millipore, Billerica, MA, USA).

MRI acquisition

MRI scans were performed using a 3T MR scanner equipped with a 32-channel head receiver coil (Philips Ingenia CX, Best, the Netherlands). The MRI protocol included T1w, T2w, FLAIR, contrast-enhanced T1w, and multi-shell diffusion imaging. Details of multi-shell diffusion imaging were as follows: axial 2D spin-echo echo planar imaging (SE-EPI) acquisition; repetition time (TR)/ echo time (TE)= 4000 ms/ 88; Flip

angle=90°; in-plane acquisition voxel size=2.5 mm×2.5 mm; acquisition matrix size=96×96; slice thickness =2.5 mm; slice number=60; b values=0, 1000, 2000 s/mm^2, with 48 motion sensitive gradient directions for each non-zero b values; SENSE factor=2; multi-band factor=3; acquisition time=6min48s. For detailed acquisition parameters, please refer to **Supplemental Table S1**.

Tumor segmentation

Tumor masks were manually delineated by two independent neuroradiologists (Y.Q. and D.C., both with three years' experience in neuroradiology) using 3DSlicer software (https://www.slicer.org/) on T2w images with T1w, FLAIR, and contrast-enhanced T1w as additional reference. A senior neuroradiologist (Y.D., with 12 years' experience in neuroradiology) reviewed and modified the tumor masks if inconsistencies between the two independent neuroradiologists (Y.Q. and D.C.) occurred or segmentation errors were observed. The overlapping areas were considered the final tumor masks.

Diffusion data preprocessing

The multi-shell diffusion images were preprocessed using a collaborative resource platform named Diffusion-MRI (https://github.com/RDadarwal/Diffusion-MRI), which incorporates DIPY (https://dipy.org/), Nipype (https://nipype.readthedocs.io/en/latest/), FSL (https://fsl.fmrib.ox.ac.uk/fsl/fslwiki/FSL), AMICO (https://github.com/daducci/AMICO) and MRtrix3 (https://www.mrtrix.org/). Image preprocessing included (1) image denoising using DIPY, (2) b0 images extraction and skull removing using FSL, (3) eddy current correction using FSL.

DKI and NODDI model fitting

The diffusion kurtosis tensor model was reconstructed using DIPY, and NODDI model was fitted using AMICO.

In total, ten diffusion metrics were calculated, including (1) fractional anisotropy (FA), (2) mean diffusivity (MD), (3) axial diffusivity (AD), (4) radial diffusivity (RD), (5) mean kurtosis (MK), (6) axial kurtosis (AK) and (7) radial kurtosis (RK), as well as (8) intracellular volume fraction (ICVF), (9) orientation dispersion index (ODI) and (10) isotropic volume fraction (ISOVF).

Tumor diffusion features extraction

The minimum, mean, median, 5th/25th/75th/95th percentiles, maximum of DKI- and NODDI-model fitted parameters were extracted within the manually segmented tumor masks as representative values.

Statistical analysis

The statistical analysis was performed using SPSS (SPSS for Windows, version 25.0; IBM, Armonk, NY, USA) and the statistics toolbox in Matlab (Matlab 2019a).

Categorical variables are presented as frequencies, and continuous variables are expressed as medians with interquartile range (IQR). Gender was compared using Chi-square test and age was compared using Mann-Whitney U test between H3 K27M-altered and wildtype gliomas. DKI- and NODDI-derived diffusion metrics were analyzed using multivariate analysis of variance (MANOVA). P-values<0.05 were considered significant.

Step-wise multivariable logistic regression was used to evaluate the discriminatory ability of clinical and diffusion parameters for H3K27M status. The area under the curve (AUC), sensitivity, specificity and accuracy were calculated.

Additionally, previous studies suggested that many BSG patients with typical MRI findings of diffuse intrinsic pontine gliomas (tDIPGs) carry H3 K27M alteration[14,15]. To incorporate an analysis by radiologists, we classified the BSGs as tDIPG or non-tDIPG based on clinical conventional MRI findings. We then explored the predictive value of tDIPG alone, and diffusion metrics combined with tDIPG for H3 K27M status.

All the statistical analyses were performed both in the whole group of BSG patients as well as in subgroups of pediatric and adult patients.

Results

Participants

Ninety-two patients with BSG were initially considered and eight patients could not be included due to poor image quality. A total of 84 patients (47 females and 37 males) were available for final analysis, of whom 56 were pediatric patients and 28 were adults. The median age at diagnosis was 10.5 (range 2-56) years in the whole group, 8 (range 2-17) years in the pediatric group and 37 (range 18-56) years in the adult group. Across all ages, 62/84 (73.8 %) patients carried an H3 K27M alteration, with a higher frequency of 82.1% (46/56) among pediatric patients compared to 57.1% (16/28) in adult patients.

Patients with H3 K27M-altered BSG were significantly younger (median 9.5 [IQR 7-18] years in alteration carriers vs. 28 [IQR 6-48] years in non-carriers, p=0.01). No gender difference was observed between H3K27M-altered and wildtype patients (F: M 34:28 vs. 13:9, p=0.81). In subgroups of pediatric and adult patients, no differences in age (8.0 [IQR 6.0-10.8] years vs. 5.5 [IQR 5.0-8.3] years, p=0.10; 35.5 [IQR 30.0-47.3] years vs. 45 [IQR 31.3-50.3] years, p=0.30) or gender (F: M 23:23 vs. 5:5, p=1; 10:5 vs. 8:4, p=1) were observed between patients with H3K27M-altered and wildtype BSGs. More than half (57.1%) of the pediatric patients presented with findings of tDIPG, while only 21.4% of the adult patients presented as tDIPG.

Detailed information is summarized in **Table 1**, and representative MRI images of the patients are shown in **Figure 1**.

Diffusion characteristics of BSG

Across all patients, the H3K27M-altered BSGs demonstrated significantly higher FA (5th percentile, 25th percentile, and median) and AK (max), but lower RD (75th

percentile) and ISOVF (25th percentile, and median) compared to H3 K27M-wildtype tumors **(Table 2) (Figure 2)**.

In the pediatric group, H3 K27M-altered cases showed significantly higher FA (5th percentile, 25th percentile, mean, median, and 75th percentile), AK (25th percentile, mean, median, 75th percentile, 95th percentile and max), MK (median, and 75th percentile), and ICVF (median). Significantly lower RD (mean, median, and 75th percentile), MD (mean, median, and 75th percentile) and ISOVF (25th percentile, mean, and median) were found in pediatric H3K27M-altered tumors **(Table 2) (Figure 2)**.

In the adult group, the H3 K27M-altered tumors showed significantly higher ICVF (5th percentile), but lower RD (75th percentile) and MD (75th percentile) **(Table 2, Figure 2)**.

Predictive value of diffusion metrics for H3K27M alteration

In the whole group, the best predictive performance for H3 K27M alteration was reached by the combination of age and median ISOVF, with an AUC of 0.78 (95%CI 0.66, 0.88) (sensitivity of 81.8%, specificity of 67.7%, accuracy of 71.4%) **(Table 3) (Figure 3)**.

In the pediatric group, the combination of median ISOVF, 5th percentile of FA, median MK, median MD showed the best predictive power, reaching an AUC of 0.91 (95%CI 0.81, 0.99) (sensitivity of 80.0%, specificity of 84.8%, accuracy of 83.9%) **(Table 3) (Figure 3)**.

In the adult group, the 75th percentile of RD demonstrated the highest diagnostic value for identifying H3 K27M alteration (AUC of 0.75 [95%CI 0.54, 0.92]), reaching a sensitivity of 75.0%, specificity of 81.3%, and accuracy of 78.6% **(Table 3) (Figure 3)**.

Moreover, we found that tDIPG alone has a high specificity but relatively low sensitivity for H3 K27M prediction (**Table S2**). A combination of diffusion metrics with tDIPG achieves a better balance of sensitivity and specificity, and improves the performance of H3 K27M alteration prediction (**Table S3**). Details of diffusion metrics of tDIPGs and non-tDIPGs are shown in **Table S4**.

Discussion

In this study, we performed a comprehensive multi-shell diffusion analysis of H3 K27M-altered and wildtype BSGs. The main findings are: (1) significant differences in diffusion metrics (FA, AK, RD, ISOVF) were identified between H3 K27M-altered and wildtype BSGs in the whole group, and additional alterations (MK, ICVF, ISOVF) were identified in the pediatric group, while only few changes were identified in the adult group (ICVF, RD, MD); (2) in the whole group, age and ISOVF together could predict the H3 K27M alteration status with an AUC of 0.78 (accuracy of 71.4%); in the pediatric group, a combination of ISOVF, FA, MK and MD metrics reached the AUC of 0.91 with high accuracy (83.9%) while a single diffusion metric (RD) reached fair performance in the adult group (AUC=0.75, accuracy of 78.6%).

In accordance with the literature, BSGs in our population were predominately found in children (56/84, 66.7%), and H3K27M alterations were more frequently detected in pediatric compared to adult patients (82.4% vs. 57.1%), suggesting that the findings of this study should be generalizable [1,16-18].

In the whole group, we found higher FA, AK and lower RD and ISOVF in H3 K27M-altered BSGs compared to H3 K27M-wildtype BSGs. FA measures the degree of diffusion anisotropy, reflecting tissue complexity and diffusivity parameters (e.g., MD and RD) measure diffusion in a single direction, reflecting the free-water movement in a particular direction, depending on tissue organization [19,20]. Previous studies suggested tumor density showed positive correlation with FA[21,22] but negative correlation with diffusivity[22] parameters. The finding of increased FA and decreased RD in our study most likely reflects increased tumor density in the H3 K27M-altered BSGs compared to the wildtype BSGs as found histopathologically[23-25]. Kurtosis measures the degree of microstructure complexity[26]. The higher AK we observed

reflects increased tissue complexity along the fiber, which could be attributed to the growth of tumor cells along fiber tracts[27-29]. Taken together, our results suggest increased tumor density and tissue complexity in H3 K27M-altered BSGs. Similarly, the increased FA, AK and decreased MD have been well recognized in IDH-wildtype gliomas[10,11,30], which are more malignant. ISOVF measures isotropic (CSF) volume fraction[31]. The decreased ISOVF found in the H3 K27M-altered tumors reflects decreased extracellular space, partially caused by higher glioma cell density or enlarged cell bodies compared to wildtype. Additionally, our previous study revealed 'fibrotic' microenvironment with reduced infiltration of immune cells in H3 K27M-altered BSG[32]. Since immunoreactive cells mediate neuroinflammation, which is likely to increase the isotropic diffusion[33], the decreased ISOVF in H3 K27M-altered BSG is expected. In the subgroups of pediatric and adult patients, the results were largely consistent with the analysis of the whole group. Additionally, increased MK, ICVF and decreased MD were identified in pediatric H3K27M-altered gliomas compared to the H3K27M wildtype BSGs. The increased MK suggests a more heterogenous microstructure, due to increased microvascular proliferation, hemorrhage, necrosis, cellularity, and structural heterogeneity[34]. Since BSGs grow in different patterns (infiltrating or expansive) and exhibit different effects (infiltration or interruption) on the fibers[35], the increased ICVF in H3 K27M -altered BSG presumably reflects infiltrating of fibers in the tumor. In the adult group, fewer diffusion metrics differed between H3K27M-altered and wildtype BSGs were identified.

When trying to predict H3K27M status, diffusion-weighted MRI provides additional diagnostic value to clinical conventional MRI. Across all patients, the combination of age and median ISOVF reached the highest performance (AUC=0.78). As previous studies suggested that pediatric BSGs are different from their adult counterparts, we also built separate models for pediatric and adult patients. In the pediatric group, the

diffusion metrics (median ISOVF, 5th percentile of FA, median MK, median MD) derived from different diffusion models (DTI, DKI, and NODDI) collectively contributed to the overall diagnostic performance (AUC=0.91) with a higher accuracy than the model for all the patients (83.9% vs. 71.4%). In the adult group, a single diffusion measure (the 75th percentile of RD) had predictive value (AUC=0.75), with an accuracy slightly higher than the model for all patients (78.6% vs. 71.4%). The differences in diffusion characteristics between pediatric and adult subgroups could be attributed to the distinct tumor microenvironment in different age groups or the developmental status of axon and myelin[36,37]. Our findings suggest that prediction of H3 K27M alteration status should be performed differently in pediatric and adult groups. A comprehensive multi-shell diffusion analysis could predict the H3 K27M alteration status with high diagnostic performance in the pediatric group. However, the diffusion metrics may not be optimal for predicting H3 K27M alteration in adult patients. Other modalities, such as amide proton transfer weighted (APTw) imaging[38], could be used to explore additional characteristics of cellular proliferation and metabolism for identifying mutation status[39,40].

Limitations

Our study was limited by the single-center design and moderate sample size. Future prospective multicenter studies are required to validate our findings. Additionally, logistic regression models were used, while a more advanced machine-learning approach (e.g., support vector machine and random forest) with more MRI features (e.g., morphology and perfusion) may further improve diagnostic performance. Third, it should be noted that NODDI provides representations of tissue complexity on the basis of technical principles and indirect results. MRI-histopathology correlation analysis is needed to validate these findings in future studies. Finally, we did not directly compare the diffusion metrics between pediatric and adult H3 K27M-altered

BSGs, as age-related effects may confound the analysis and no healthy controls were available for comparison.

Conclusions

Different alterations patterns of diffusion measures (e.g., FA, MK, and ICVF) were identified between H3 K27M-altered and wildtype BSGs, being more prominent in the pediatric subgroup. A model using metrics derived from multi-shell analysis had excellent predictive value for H3 K27M alteration status in pediatric patients, while only fair predictive power in adult patients.

Funding:

Y.L is supported by the National Science Foundation of China (Nos. 81870958), the Beijing Municipal Natural Science Foundation for Distinguished Young Scholars (No. JQ20035), the Special Fund of the Pediatric Medical Coordinated Development Center of Beijing Hospitals Authority (No. XTYB201831).

F.B is supported by the NIHR biomedical research center at UCLH.

Conflict of Interest: All authors reported no competing interests.

References

1. Ostrom QT, Price M, Neff C, et al. CBTRUS Statistical Report: Primary Brain and Other Central Nervous System Tumors Diagnosed in the United States in 2015-2019. *Neuro Oncol.* 2022; 24(Suppl 5):v1-v95.

2. Guillamo JS, Monjour A, Taillandier L, et al. Brainstem gliomas in adults: prognostic factors and classification. *Brain.* 2001; 124(Pt 12):2528-2539.

3. Meyronet D, Esteban-Mader M, Bonnet C, et al. Characteristics of H3 K27M-mutant gliomas in adults. *Neuro Oncol.* 2017; 19(8):1127-1134.

4. Liu Z, Feng S, Li J, et al. The Epidemiological Characteristics and Prognostic Factors of Low-Grade Brainstem Glioma: A Real-World Study of Pediatric and Adult Patients. *Front Oncol.* 2020; 10:391.

5. Louis DN, Perry A, Wesseling P, et al. The 2021 WHO Classification of Tumors of the Central Nervous System: a summary. *Neuro Oncol.* 2021; 23(8):1231-1251.

6. Karremann M, Gielen GH, Hoffmann M, et al. Diffuse high-grade gliomas with H3 K27M mutations carry a dismal prognosis independent of tumor location. *Neuro Oncol.* 2018; 20(1):123-131.

7. Raab P, Hattingen E, Franz K, Zanella FE, Lanfermann H. Cerebral gliomas: diffusional kurtosis imaging analysis of microstructural differences. *Radiology.* 2010; 254(3):876-881.

8. Miller P, Coope D, Thompson G, Jackson A, Herholz K. Quantitative evaluation of white matter tract DTI parameter changes in gliomas using nonlinear registration. *Neuroimage.* 2012; 60(4):2309-2315.

9. Wen Q, Kelley DA, Banerjee S, et al. Clinically feasible NODDI characterization of glioma using multiband EPI at 7 T. *Neuroimage Clin.* 2015; 9:291-299.

10. Zhao J, Wang YL, Li XB, et al. Comparative analysis of the diffusion kurtosis imaging and diffusion tensor imaging in grading gliomas, predicting tumour cell proliferation and IDH-1 gene mutation status. *J Neurooncol.* 2019; 141(1):195-203.

11. Figini M, Riva M, Graham M, et al. Prediction of Isocitrate Dehydrogenase Genotype in Brain Gliomas with MRI: Single-Shell versus Multishell Diffusion Models. *Radiology.* 2018; 289(3):788-796.

12. Zhao J, Li JB, Wang JY, et al. Quantitative analysis of neurite orientation dispersion and density imaging in grading gliomas and detecting IDH-1 gene mutation status. *Neuroimage Clin.* 2018; 19:174-181.

13. Louis DN, Perry A, Reifenberger G, et al. The 2016 World Health Organization Classification of Tumors of the Central Nervous System: a summary. *Acta Neuropathol.* 2016; 131(6):803-820.

14. Walker DA, Liu J, Kieran M, et al. A multi-disciplinary consensus statement concerning surgical approaches to low-grade, high-grade astrocytomas and diffuse intrinsic pontine gliomas in childhood (CPN Paris 2011) using the Delphi method. *Neuro Oncol.* 2013; 15(4):462-468.

15. Chiang J, Diaz AK, Makepeace L, et al. Clinical, imaging, and molecular analysis of pediatric pontine tumors lacking characteristic imaging features of DIPG. *Acta Neuropathol Commun.* 2020; 8(1):57.

16. Ostrom QT, Patil N, Cioffi G, Waite K, Kruchko C, Barnholtz-Sloan JS. CBTRUS Statistical Report: Primary Brain and Other Central Nervous System Tumors Diagnosed in the United States in 2013-2017. *Neuro Oncol.* 2020; 22(12 Suppl 2):iv1-iv96.

17. Wu G, Broniscer A, McEachron TA, et al. Somatic histone H3 alterations in pediatric diffuse intrinsic pontine gliomas and non-brainstem glioblastomas. *Nat Genet.* 2012; 44(3):251-253.

18. Feng J, Hao S, Pan C, et al. The H3.3 K27M mutation results in a poorer prognosis in brainstem gliomas than thalamic gliomas in adults. *Hum Pathol.* 2015; 46(11):1626-1632.

19. Tabesh A, Jensen JH, Ardekani BA, Helpern JA. Estimation of tensors and tensor-derived measures in diffusional kurtosis imaging. *Magn Reson Med.* 2011; 65(3):823-836.

20. Wheeler-Kingshott CA, Ciccarelli O, Schneider T, Alexander DC, Cercignani M. A new approach to structural integrity assessment based on axial and radial diffusivities. *Funct Neurol.* 2012; 27(2):85-90.

21. Beppu T, Inoue T, Shibata Y, et al. Measurement of fractional anisotropy using diffusion tensor MRI in supratentorial astrocytic tumors. *J Neurooncol.* 2003; 63(2):109-116.

22. Kinoshita M, Hashimoto N, Goto T, et al. Fractional anisotropy and tumor cell density of the tumor core show positive correlation in diffusion tensor magnetic resonance imaging of malignant brain tumors. *Neuroimage.* 2008; 43(1):29-35.

23. Buczkowicz P, Bartels U, Bouffet E, Becher O, Hawkins C. Histopathological spectrum of paediatric diffuse intrinsic pontine glioma: diagnostic and therapeutic implications. *Acta Neuropathol.* 2014; 128(4):573-581.

24. Wang L, Li Z, Zhang M, et al. H3 K27M-mutant diffuse midline gliomas in different anatomical locations. *Hum Pathol.* 2018; 78:89-96.

25. Solomon DA, Wood MD, Tihan T, et al. Diffuse Midline Gliomas with Histone H3-K27M Mutation: A Series of 47 Cases Assessing the Spectrum of Morphologic Variation and Associated Genetic Alterations. *Brain Pathol.* 2016; 26(5):569-580.

26. Jensen JH, Helpern JA, Ramani A, Lu H, Kaczynski K. Diffusional kurtosis imaging: the quantification of non-gaussian water diffusion by means of magnetic resonance imaging. *Magn Reson Med.* 2005; 53(6):1432-1440.

27. Giese A, Kluwe L, Laube B, Meissner H, Berens ME, Westphal M. Migration of human glioma cells on myelin. *Neurosurgery.* 1996; 38(4):755-764.

28. Mabray MC, Glastonbury CM, Mamlouk MD, Punch GE, Solomon DA, Cha S. Direct Cranial Nerve Involvement by Gliomas: Case Series and Review of the Literature. *AJNR Am J Neuroradiol.* 2015; 36(7):1349-1354.

29. Barajas RF, Jr., Hess CP, Phillips JJ, et al. Super-resolution track density imaging of glioblastoma: histopathologic correlation. *AJNR Am J Neuroradiol.* 2013; 34(7):1319-1325.

30. Kim SH, Kim H, Kim TS. Clinical, histological, and immunohistochemical features predicting 1p/19q loss of heterozygosity in oligodendroglial tumors. *Acta Neuropathol.* 2005; 110(1):27-38.

31. Zhang H, Schneider T, Wheeler-Kingshott CA, Alexander DC. NODDI: practical in vivo neurite orientation dispersion and density imaging of the human brain. *Neuroimage.* 2012; 61(4):1000-1016.

32. Xiao X, Li X, Wang Y, et al. Classification of Brainstem Gliomas Based on Tumor Microenvironment Status. *Cancers (Basel).* 2023; 15(17).

33. Schwartz M, Butovsky O, Bruck W, Hanisch UK. Microglial phenotype: is the commitment reversible? *Trends Neurosci.* 2006; 29(2):68-74.

34. Hempel JM, Bisdas S, Schittenhelm J, et al. In vivo molecular profiling of human glioma using diffusion kurtosis imaging. *J Neurooncol.* 2017; 131(1):93-101.

35. Pan C, Zhang M, Xiao X, et al. A multimodal imaging-based classification for pediatric diffuse intrinsic pontine gliomas. *Neurosurg Rev.* 2023; 46(1):151.

36. Slater DA, Melie-Garcia L, Preisig M, Kherif F, Lutti A, Draganski B. Evolution of white matter tract microstructure across the life span. *Hum Brain Mapp.* 2019; 40(7):2252-2268.

37. Grinberg F, Maximov, II, Farrher E, et al. Diffusion kurtosis metrics as biomarkers of microstructural development: A comparative study of a group of children and a group of adults. *Neuroimage.* 2017; 144(Pt A):12-22.

38. Zhou J, Zhu H, Lim M, et al. Three-dimensional amide proton transfer MR imaging of gliomas: Initial experience and comparison with gadolinium enhancement. *J Magn Reson Imaging.* 2013; 38(5):1119-1128.

39. Joo B, Han K, Ahn SS, et al. Amide proton transfer imaging might predict survival and IDH mutation status in high-grade glioma. *Eur Radiol.* 2019; 29(12):6643-6652.

40. Park JE, Kim HS, Park KJ, Kim SJ, Kim JH, Smith SA. Pre- and Posttreatment Glioma: Comparison of Amide Proton Transfer Imaging with MR Spectroscopy for Biomarkers of Tumor Proliferation. *Radiology.* 2016; 278(2):514-523.

Table 1 Characteristics of all the participants with brainstem gliomas.

		All patients (n=84)	Pediatric patients (n=56)	Adult patients (n=28)
Age (median, IQR) (y.o.)		10.5(6.8-30.0)	8.0(5.0-10.3)	37.0(30.0-49.0)
Gender	F: M	47:37	28:28	19:9
Conventional MRI characteristics				
	Location (num,%)			
	Midbrain	14(16.7%)	6(10.7%)	8(28.6%)
	Pons	65(77.4%)	49(87.5%)	16(57.1%)
	Medulla	10(11.9%)	5(8.9%)	5(17.9%)
	Dorsal exophytic component	11(13.1%)	6(10.7%)	5(17.9%)
	Hydrocephalus	20(23.8%)	11(19.6%)	9(32.1%)
	Cystic component	37(44.0%)	31(55.4%)	6(21.4%)
	Contrast enhancement	51(60.7%)	39(69.6%)	12(42.9%)
	Engulfment of basilar artery	48(57.1%)	39(69.6%)	9(32.1%)
	tDIPG	38 (45.2%)	32 (57.1%)	6 (21.4%)
WHO grading (num,%)	I-II	21 (25.0%)	11(19.6%)	10 (35.7%)
	III	9 (10.7%)	4(7.2%)	5 (17.9%)
	IV	54 (64.3%)	41(73.2%)	13 (46.4%)
H3K27M alteration status	WT: altered	22:62	10:46	12:16

Abbreviations: IQR=interquartile range; num=number; tDIPG = typical diffuse intrinsic pontine glioma; WT=wildtype.

Table 2 Comparison of multi-shell diffusion metrics between H3K27M wildtype and altered BSGs.

	H3K27M wildtype	H3K27M-altered	p value*
All participants			
FA_{5th}	0.09 (0.08-0.11)	0.10 (0.09-0.12)	0.03
FA_{25th}	0.16 (0.12-0.19)	0.17 (0.15-0.20)	0.02
FA_{Median}	0.23 (0.18-0.27)	0.25 (0.21-0.27)	0.03
RD_{75th} ($\times10^{-3}mm^2/s$)	1.77 (1.47-1.89)	1.53 (1.29-1.72)	0.03
AK_{Max}	1.35 (1.23-1.68)	2.03 (1.48-2.55)	0.03
$ISOVF_{25th}$	0.15 (0.09-0.20)	0.10 (0.06-0.13)	0.02
$ISOVF_{Median}$	0.29 (0.17-0.40)	0.20 (0.13-0.27)	0.01
Pediatric group			
FA_{5th}	0.08 (0.07-0.10)	0.10 (0.09-0.12)	0.006
FA_{25th}	0.14 (0.12-0.17)	0.17 (0.15-0.20)	0.006
FA_{Mean}	0.23 (0.30-0.25)	0.26 (0.23-0.28)	0.01
FA_{Median}	0.20 (0.17-0.23)	0.24 (0.21-0.27)	0.007
FA_{75th}	0.29 (0.25-0.32)	0.32 (0.29-0.36)	0.02
MD_{Mean} ($\times10^{-3}mm^2/s$)	1.76 (1.66-1.99)	1.67 (1.50-1.77)	0.03
MD_{Median} ($\times10^{-3}mm^2/s$)	1.73 (1.64-2.01)	1.50 (1.34-1.67)	0.02
MD_{75th} ($\times10^{-3}mm^2/s$)	1.94 (1.91-2.23)	1.82 (1.61-1.92)	0.02
RD_{Mean} ($\times10^{-3}mm^2/s$)	1.57 (1.51-1.79)	1.43 (1.28-1.55)	0.01
RD_{Median} ($\times10^{-3}mm^2/s$)	1.59 (1.45-1.81)	1.32 (1.21-1.45)	0.009
RD_{75th} ($\times10^{-3}mm^2/s$)	1.81 (1.74-2.07)	1.61 (1.41-1.76)	0.009
MK_{Median}	0.47 (043-0.50)	0.52 (0.47-0.58)	0.03
MK_{75th}	0.55 (0.53-0.59)	0.64 (0.58-0.69)	0.03
AK_{25th}	0.40 (0.38-0.44)	0.44 (0.42-0.48)	0.02
AK_{Mean}	0.49 (0.46-0.52)	0.53 (0.51-0.61)	0.01
AK_{Median}	0.47 (0.44-0.49)	0.51(0.49-0.57)	0.01
AK_{75th}	0.55 (0.52-0.57)	0.61 (0.58-0.69)	0.01
AK_{95th}	0.72 (0.67-0.77)	0.79 (0.74-0.96)	0.03
AK_{Max}	1.28 (1.21-1.68)	2.14 (1.55-2.55)	0.007
$ICVF_{Median}$	0.17 (0.11-0.18)	0.22 (0.18-0.27)	0.04
$ISOVF_{25th}$	0.19 (0.12-0.27)	0.11 (0.08-0.13)	0.003
$ISOVF_{Mean}$	0.37 (0.31-0.47)	0.27 (0.24-0.36)	0.02
$ISOVF_{Median}$	0.33 (0.24-0.43)	0.22 (0.17-0.28)	0.003
Adult group			
MD_{75th} ($\times10^{-3}mm^2/s$)	1.68 (1.42-2.01)	1.35 (1.16-1.52)	0.02
RD_{75th} ($\times10^{-3}mm^2/s$)	1.49 (1.27-1.87)	1.20 (1.01-1.33)	0.02
$ICVF_{5th}$	0.14 (0.10-0.18)	0.20 (0.14-0.25)	0.04

Abbreviations: FA = fractional anisotropy; MD = mean diffusivity; RD= radial diffusivity; AK = axial kurtosis; ISOVF = isotropic volume fraction; MK = mean kurtosis; ICVF = intracellular volume fraction; Max = maximum; Min = minimum.
*showing diffusion metrics with $p<0.05$

Table 3. Performance of BSG multi-shell diffusion metrics for predicting H3K27M alteration status.

Parameter	Sensitivity (95% CI)	Specificity (95% CI)	Accuracy (95% CI)	AUC (95% CI)	OR (95% CI)	p value
All participants						
Age	81.8% (51.6%, 89.9%)	67.7% (58.3%, 100%)	71.4% (60.7%, 84.5%)	0.78 (0.66, 0.88)	-0.057 (-0.070, -0.048)	0.002
$ISOVF_{Median}$					-7.94 (-9.87, -6.73)	0.002
Pediatric group						
$ISOVF_{Median}$	80.0% (57.6%, 100%)	84.8% (70%, 100%)	83.9% (64.3%, 98.2%)	0.91 (0.81, 0.99)	-15.64 (-21.90, 9,11)	0.009
FA_{5th}					7.18 (-3.63, 9.70)	0.015
MK_{Median}					86.61 (74.01, 120.61)	0.020
MD_{Median}					36.93 (31.35, 54.94)	0.031
Adult group						
RD_{75th}	75.0% (40.5%, 100%)	81.3% (43.8%, 100%)	78.6% (64.3%, 92.9%)	0.75 (0.54, 0.92)	-2.73 (-3.83, -2.18)	0.036

Abbreviations: AUC = area under the curve; CI= confidence interval; ISOVF = isotropic volume fraction; FA = fractional anisotropy; MK = mean kurtosis; MD = mean diffusivity; RD= radial diffusivity.

Figure Legends

Figure 1. Representative T2-weighted images, colored multi-shell diffusion parameter maps, and tractography of patients with H3K27M-altered and wildtype BSGs.

Tumors are shown in purple mask on T2w images. The median and IQR of representative diffusion metric (FA/MK/ICVF) from multi-shell diffusion models （DTI/DKI/NODDI）and the tractography images are listed on the corresponding map. **First row**: a 32 years old female with H3K27M-altered BSG. **Second row**: a 28 years old female with H3K27M-wildtype BSG. **Third row**: a 12 years old male with H3K27M-altered BSG. **Forth row**: a 9 years old female with H3K27M-wildtype BSG.

Abbreviations: BSG= brainstem glioma; FA = fractional anisotropy; MK = mean kurtosis; ICVF = intracellular volume fraction; IQR= interquartile range.

Note: The range of MK color bar was set as 0-2 to highlight the differences between tumors and surrounding structures. The orientation of the tracts was adjusted to visualize the relationship between the tracts and the BSGs.

Figure 2. Representative box plots of multi-shell diffusion metrics of H3 K27M-altered and wildtype BSGs of all patients and subgroups of pediatric and adult patients.

Abbreviations: FA = fractional anisotropy; AK = axial kurtosis; ISOVF = isotropic volume fraction; MD = mean diffusivity; RD= radial diffusivity, ICVF = intracellular volume fraction.

Figure 3. ROC of H3 K27M alteration prediction model based on diffusion metrics in BSGs of all patients and subgroups of pediatric and adult patients.

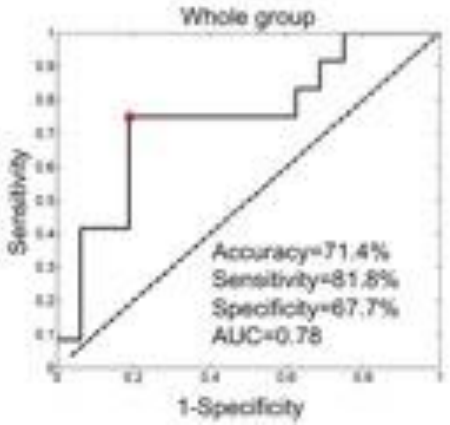
Whole group
Sensitivity
1-Specificity
Accuracy=71.4%
Sensitivity=81.8%
Specificity=67.7%
AUC=0.78

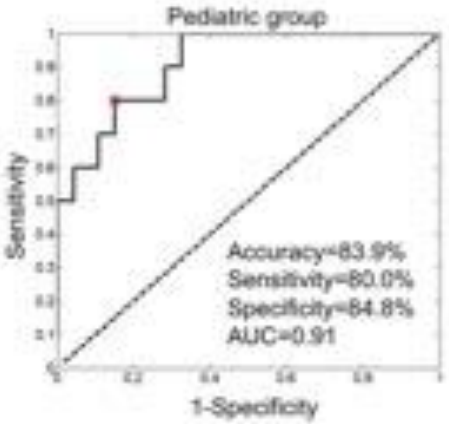
Pediatric group
Sensitivity
1-Specificity
Accuracy=83.9%
Sensitivity=80.0%
Specificity=84.8%
AUC=0.91

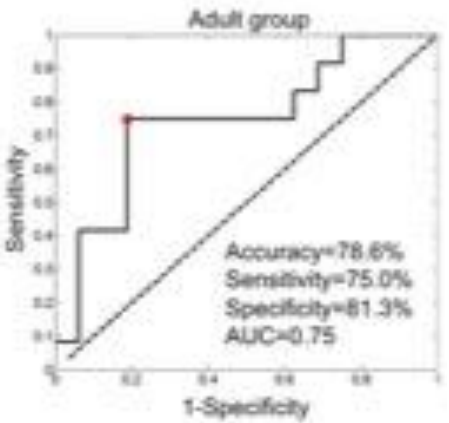
Adult group
Sensitivity
1-Specificity
Accuracy=78.6%
Sensitivity=75.0%
Specificity=81.3%
AUC=0.75

whole group

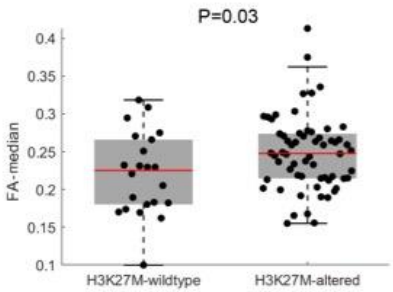

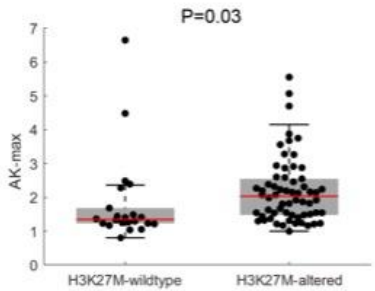

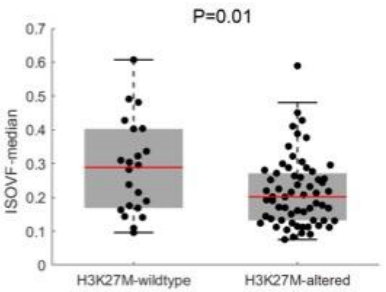

pediatric group

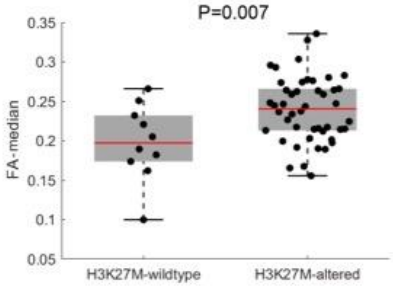

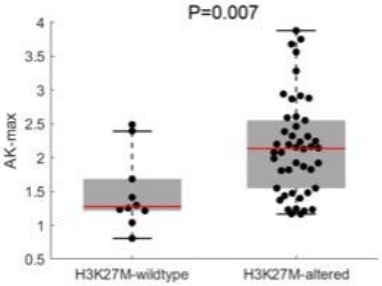

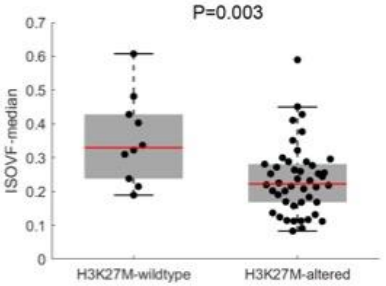

adult group

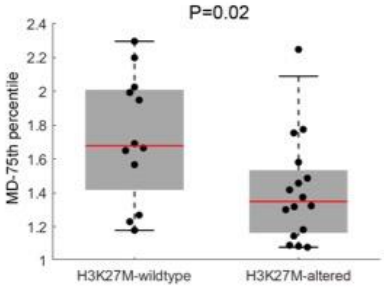

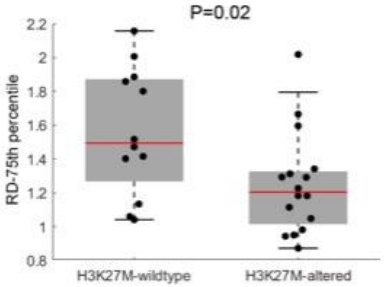

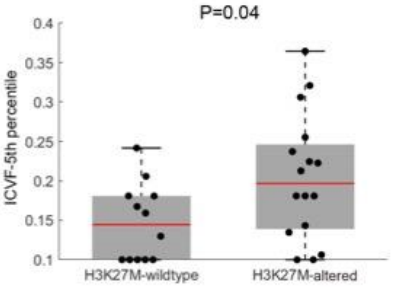

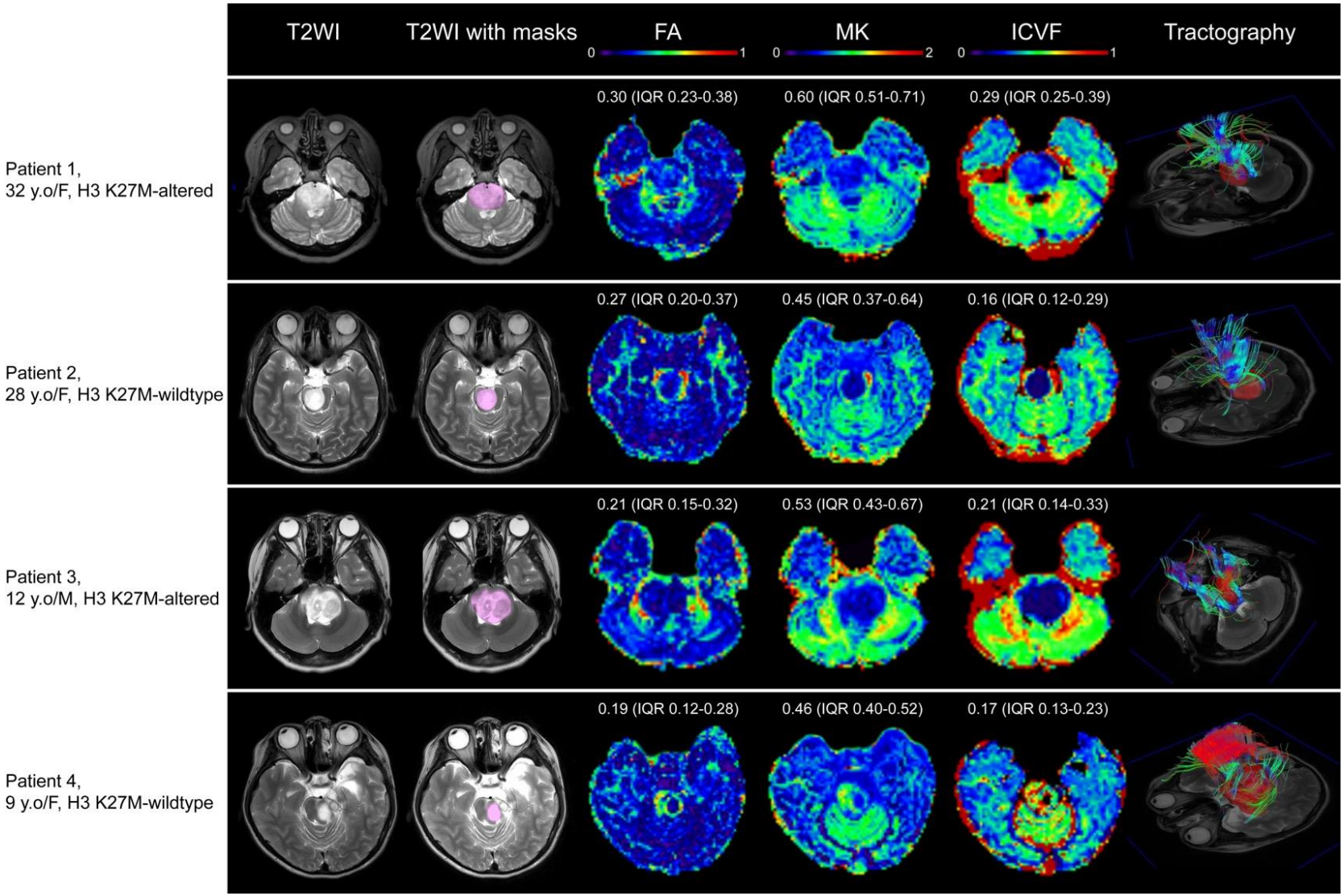
T2WI
T2WI with masks
FA
0
1
MK
0
2
ICVF
0
1
Tractography
Patient 1,
32 y.o/F, H3 K27M-altered
0.30 (IQR 0.23-0.38)
0.60 (IQR 0.51-0.71)
0.29 (IQR 0.25-0.39)
Patient 2,
28 y.o/F, H3 K27M-wildtype
0.27 (IQR 0.20-0.37)
0.45 (IQR 0.37-0.64)
0.16 (IQR 0.12-0.29)
Patient 3,
12 y.o/M, H3 K27M-altered
0.21 (IQR 0.15-0.32)
0.53 (IQR 0.43-0.67)
0.21 (IQR 0.14-0.33)
Patient 4,
9 y.o/F, H3 K27M-wildtype
0.19 (IQR 0.12-0.28)
0.46 (IQR 0.40-0.52)
0.17 (IQR 0.13-0.23)

Table S1. **MRI acquisition parameters of T1w, T2w, FLAIR and contrast-enhanced T1w**

Protocols	Sequence	FA (degree)	TR (ms)	TE (ms)	IR (ms)	Acquisition voxel size (mm^3)	In-plane acquisition matrix	Slice number	Acquisition time
T1w (sag)	3D TFE	8	6.6	3		1×1×1	256×256	196	2min20s
T2w (ax)	2D TSE	90	2800	135		1×1×5 (gap 0.5mm)	240×240	24	1min
T2-FLAIR (sag)	3D TSE	90	4800	340	1605	1×1×1	240×240	180	2min28s
Contrast-enhanced T1w (sag)	3D TFE	8	6.6	3		1×1×1	256×256	196	2min20s

Abbreviations: FA= flip angle; TR= repetition time; TE= echo time; IR= inversion recovery; FLAIR= fluid attenuated inversion recovery; TFE= turbo field echo; TSE= turbo spin echo; sag= sagittal; ax= axial.

Table S2. Predictive value of tDIPG for H3K27M alteration

	Sensitivity	Specificity	AUC
All participants	0.60	0.95	0.76
Pediatric group	0.67	0.89	0.74
Adult group	0.38	1.00	0.69

Abbreviations: tDIPG = typical diffuse intrinsic pontine glioma

Table S3. Predictive value of diffusion metrics combined with tDIPG for H3K27M alteration

	Sensitivity	Specificity	AUC
All participants	0.84	0.80	0.86
Pediatric group	0.93	0.89	0.95
Adult group	0.88	0.73	0.83

Abbreviations: tDIPG = typical diffuse intrinsic pontine glioma

Table S4 Diffusion metrics of tDIPG and non-DIPG

	tDIPG	Non-DIPG	p value*
All participants			
FA_{median}	0.26 (0.22-0.28)	0.23 (0.19-0.27)	0.01
FA_{25th}	0.18 (0.16-0.20)	0.16 (0.14-0.19)	0.02
MD_{5th}	1.07 (0.92-1.17)	0.96 (0.87-1.02)	0.04
ODI_{mean}	0.22 (0.19-0.27)	0.27 (0.23-0.33)	0.01
ODI_{median}	0.19 (0.16-0.23)	0.24 (0.20-0.29)	<0.001
ODI_{25th}	0.10 (0.09-0.12)	0.15 (0.10-0.21)	<0.001
ODI_{75th}	0.29 (0.25-0.34)	0.33 (0.29-0.39)	0.02
Pediatric group			
FA_{mean}	0.27 (0.24-0.29)	0.24 (0.22-0.26)	0.01
FA_{median}	0.25 (0.22-0.28)	0.21 (0.19-0.23)	0.002
FA_{5th}	0.11 (0.09-0.13)	0.09 (0.08-0.10)	0.004
FA_{25th}	0.18 (0.15-0.20)	0.15 (0.14-0.17)	0.002
FA_{75th}	0.33 (0.30-0.35)	0.30 (0.27-0.33)	0.02
AK_{Max}	2.17 (1.85-2.60)	1.51 (1.24-2.20)	0.01
ODI_{median}	0.19 (0.16-0.23)	0.21 (0.19-0.28)	0.03
ODI_{25th}	0.10 (0.09-0.12)	0.12 (0.10-0.18)	0.01
Adult group			
FA_{75th}	0.38 (0.36-0.44)	0.34 (0.31-0.37)	0.03
MD_{min} ($\times 10^{-3} mm^2/s$)	0.41 (0.35-0.61)	0.63 (0.56-0.69)	0.01
RD_{min} ($\times 10^{-3} mm^2/s$)	0.13 (0.10-0.19)	0.29 (0.22-0.39)	0.003
RK_{mean}	1.03 (0.77-1.24)	0.68 (0.62-0.77)	0.001
ODI_{25th}	0.10 (0.08-0.14)	0.16 (0.12-0.23)	0.03

Abbreviations: tDIPG = typical diffuse intrinsic pontine glioma; FA = fractional anisotropy; MD = mean diffusivity; ODI= orientation dispersion index; AK = axial kurtosis; RD= radial diffusivity; RK = radial kurtosis; ICVF = intracellular volume fraction; min = minimum.

Table S5 Correlation analysis of contrast-enhancement and diffusion metrics

	Non-enhancement	Contrast-enhancement	p value*
All participants			
RD_{95th} ($\times10^{-3}mm^2/s$)	2.03 (1.71-2.29)	2.32 (1.91-2.78)	0.03
ODI_{Mean}	0.23 (0.19-0.25)	0.26 (0.20-0.31)	0.02
ODI_{95th}	0.50 (0.41-0.59)	0.58 (0.46-1.00)	0.01
$ISOVF_{75th}$	0.30 (0.26-0.37)	0.38 (0.31-0.55)	0.03
Pediatric group			
MD_{95th} ($\times10^{-3}mm^2/s$)	2.29 (1.96-2.47)	2.64 (2.26-3.19)	0.03
RD_{95th} ($\times10^{-3}mm^2/s$)	2.08 (1.75-2.28)	2.32 (1.99-2.88)	0.03
AD_{95th} ($\times10^{-3}mm^2/s$)	2.72 (2.44 -3.11)	3.11 (2.80-3.93)	0.04
Adult group			
AD_{25th} ($\times10^{-3}mm^2/s$)	1.59 (1.54-1.76)	1.36 (1.30-1.43)	0.03
AK_{Max}	2.28 (1.54-5.44)	1.41 (1.30-1.68)	0.03
ODI_{25th}	0.13 (0.09-0.14)	0.16 (0.12-0.24)	0.04

Abbreviations: RD= radial diffusivity; ODI= orientation dispersion index; ISOVF = isotropic volume fraction; MD = mean diffusivity; AD = axial diffusivity; AK = axial kurtosis.

Table S6 Diffusion metrics of the corticospinal tract in the cerebral peduncle

	BSG patients	Healthy Controls	p value*
FA	0.61 (0.56-0.64)	0.45 (0.40-0.48)	<0.001
RD ($\times10^{-3}mm^2/s$)	0.67 (0.62-0.72)	1.06 (0.91-1.19)	<0.001
MD ($\times10^{-3}mm^2/s$)	1.10 (1.01-1.06)	1.42 (1.26-1.52)	0.003
ISOVF	0.22 (0.16-0.24)	0.31(0.24-0.36)	0.01

Table S7 Diffusion metrics of the corticospinal tract in the posterior limb of the internal capsule

	BSG patients	Healthy Controls	p value*
AK	0.73 (0.68-0.77)	0.81 (0.77-0.86)	<0.001
AD ($\times10^{-3}mm^2/s$)	1.56 (1.50-1.59)	1.42 (1.35-1.48)	<0.001
MD ($\times10^{-3}mm^2/s$)	0.84 (0.81-0.80)	0.78 (0.20-0.84)	0.003